Nuclear Instruments and Methods in Physics Research 228 (1984) 193–200
North-Holland, Amsterdam

DIGITAL IMAGING WITH A PRESSURIZED XENON FILLED MWPC WORKING AT A HIGH DATA RATE

R. BELLAZZINI, A. BREZ, A. DEL GUERRA, M.M. MASSAI and M.R. TORQUATI

Dipartimento di Fisica dell'Università di Pisa and INFN, Sezione di Pisa, Piazza Torricelli, 2-I-56100 Pisa, Italy

M. FRANCHI and G. PERRI

Istituto di Radiologia dell'Università di Pisa, Via Roma, 2-I-56100 Pisa, Italy

Received 21 March 1984 and in revised form 12 June 1984

A MWPC based detection system for medical imaging is presented. The system consists of a pressurized Xenon filled MWPC and of a monochromatic, fluorescent, X-ray source using a conventional diagnostic tube with various target/filter combinations. The main performance of the system are: 10% efficiency, 30% energy resolution, 500 μm spatial resolution, ± 5 uniformity. The preliminary results of the application of this system to bone densitometry are presented.

1. Introduction

In the last ten years the field of medical imaging has been revolutionized by the introduction of new methodologies (CAT, Digital Radiography, NMR, etc) combined with powerful digital techniques. This process has been made more attractive by the drastic drop of the cost of computer hardware and, particularly, of RAM and ROM memories. On the other hand, the field of medical radiation detectors has remained more steady. Almost all of the existing devices are still of the integrating type, which are often hampered by linearity, noise or dynamic range problems. In this respect, a detection system counting individual photons should have several advantages: i) low noise, given by definition by the photon statistics; ii) high linearity and dynamic range limited only by dead-time losses (which can be accounted for). A MWPC is a Poissonian electronic, area detector and for this reason since its introduction it has received great attention for its possible application in the biomedical field. However, to be suitable for medical imaging a MWPC should satisfy the following stringent requirements: 1) good detection efficiency; 2) good spatial resolution; 3) high-rate capability. To satisfy the first requirement one has to use a gas with a high atomic number (xenon), possibly at high pressure. For the second requirement, the use of a monochromatic X-ray source with energy just above the K-edge of xenon ($= 34.6$ keV) can greatly help to achieve a submillimeter spatial resolution [1]. Until a few years ago, the speed of the electronic data acquisition system was the most severe bottleneck for the solution of the third problem. The recent introduction of very fast TDCs and of histogramming memories has greatly simplified the problem, allowing to reach a data capability of more than 1 MHz in a straightforward way. The modern generation of MWPCs seems to be competitive with the existing imaging devices, especially when quantitative studies on stationary objects must be performed (i.e. bone or lung densitometry).

In this paper we present the results obtained with a MWPC detection system and a monochromatic X-ray source specially designed for medical imaging. The preliminary results of the application of this system to bone densitometry are also presented.

2. The monochromatic X-ray source

A quantitative study of radiation transmission through matter requires the use of a monochromatic source. Important parameters like attenuation coefficient, thickness, or mass can be measured only by using a source with a well defined energy. Furthermore, it is well accepted that the use of a monochromatic source maximizes the image contrast per unit absorbed dose. Unfortunately, the use of a radioactive γ-source is counteracted by the unavailability of sources of sufficient strength in the energy interval (30–50 keV) of practical interest. A significant exception is gadolinium (^{153}Gd) which emits the fluorescent X-rays of its decay product ^{153}Eu ($E\gamma = 41.5$ keV).

This source, however, has some disadvantages: i) it is expensive; ii) its half-live is only 241 d; iii) from a

radioprotection point of view it is not very easy to handle a source of several hundreds of mCi. To overcome these problems we have developed a monochromatic, fluorescent, X-ray source by using a conventional tube with targets and filters of various elements [2]. The advantages of this solution are: i) it is inexpensive because an X-ray generator is available in every diagnostic center; ii) the energy of the source can be selected by simply modifying the target–filter combination; iii) patient and operator exposure is limited to the examination time. A scheme of the fluorescent X-ray source is shown in fig. 1. A fluorescent target is placed at an angle 45° relative to the primary beam from the diagnostic X-ray tube. The entrance aperture determines the fraction of the fluorescent target irradiated, and thus the area and size of the fluorescent X-ray source. The detector is exposed to the fluorescent X-rays which pass first through a filter and then through the exit aperture. The filter material, with a K absorption edge between the K_α and K_β lines of the target, removes most of the K_β as well as the scattered radiation.

Consequently, nearly monoenergetic K_α X-rays are obtained. The exit aperture defines the size and the shape of the radiation pattern. The whole system was carefully alligned with a laser beam. For the selection of three different X-ray energies (40, 42 and 45 keV), we have used three combinations of four elements (samarium, neodymium, dysprosium and gadolinium) for the target and filter (see table 1). The target was a foil 25 mm × 25 mm with a thickness of 700 μm.

The spectra generated from a samarium target with and without the neodymium filter are shown in fig. 2a and in fig. 2b respectively. The spectrum was measured with a high energy resolution germanium detector. The use of the neodymium filter reduces the number of the K_β X-rays from the samarium target and improves the purity of the beam. The spectrum shown contains ≃ 96% K_α X-rays; it is, therefore, highly monoenergetic. The flux incident on the whole chamber placed at a distance of 70 cm from the target was ≃ 2×10^6 photons/second. The X-ray tube used for these measurements was a very simple, portable, instrument with half-wave rectification

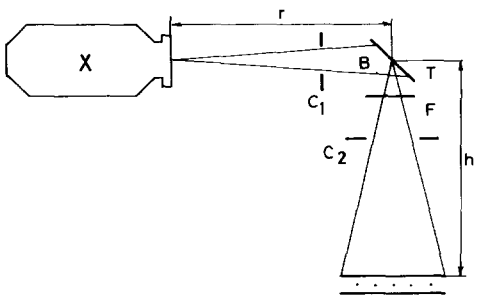

Fig. 1. A scheme of the fluorescent X-ray source: C1: entrance collimator, C2: exit collimator, T: target, F: filter.

Table 1
X-ray energy selection.

Target	samarium	gadolinium	dysprosium
Filter	neodymium	samarium	gadolinium
Energy	40 keV	42 keV	45 keV

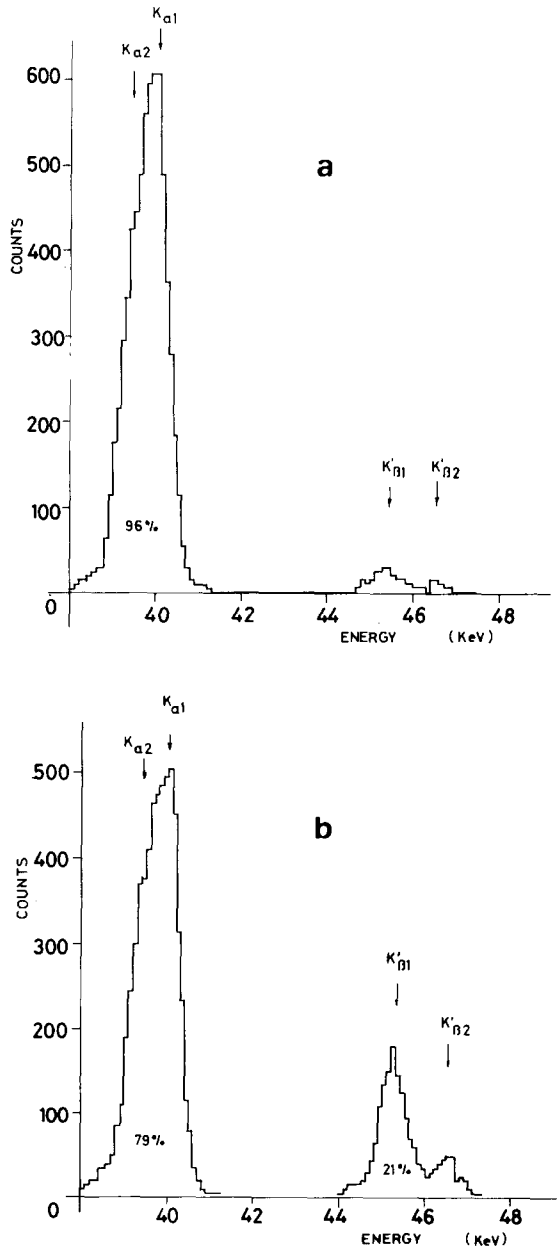

Fig. 2. (a) Spectrum generated by a samarium target with the neodymium filter, (b) the same as (a), without neodymium filter.

and a current limit of 5 mA at the maximum accelerating voltage of 80 kV. A flux greater by at least one order of magnitude can be obtained by using a modern three-phase X-ray generator with full-wave rectification, 110–120 kVp and a current output of 10 mA. If we assume a 10% detection efficiency and, for example, a 20% X-ray transmission through an arm we can estimate a data rate of $\simeq 10^6$ counts/second that corresponds well to the speed of the electronic data acquisition system (see sect. 4). It should be noted that an equivalent data rate could be obtained with a ^{153}Gd source of, at least, 1 Ci strength.

3. The MWPC

The chamber we built is a thin chamber (6.4 mm total active thickness). The advantages of a thin chamber design are: i) reduced parallax error (< 400 μm at maximum in our case); ii) high signal to noise ratio, because of the increase of the charge induced on the cathodes relative to the avalanche charge [3]. To counteract the decrease of efficiency we built a chamber that could be operated at pressures of up to four atmospheres. Increasing the pressure gives the further advantage of reducing the range of the photo- and Auger-electrons thus improving the spatial resolution and allowing for the use of sources with higher energies (up to $\simeq 70$ keV). The main geometrical parameters of the MWPC are listed in table 2. When working with a pressurized chamber a crucial point is the design of the window which must be sturdy and, at the same time, transparent to the incoming radiation. We have solved this problem with a window made up of a sandwich of a very light material with a high resistance to compression (Rohacell 71, 0.071 g/cm^3 density, 1 cm thick) and two foils of a material with a high tensile strength (vetronite, 1.8 g/cm^3 density, 200 μm thick). This type of window has an equivalent mass density of 0.18 g/cm^2 corresponding to $\simeq 700$ μm of aluminum. It absorbs less than 5% of the incoming radiation at 40 keV and its maximum sag at 3 atm is only 600 μm. The area of the chamber (128 mm $\times$ 128 mm) was selected to fit the present size of the CAMAC memory (128 $\times$ 256 pixels). The spatial sampling is therefore 0.5 mm in the direction parallel to the anode wires and 1 mm in the orthogonal direction. The two cathodes consist of 2.7 mm wide strips deposited on a printed circuit board of 200 μm thickness. The ratio of 0.8 between the width of the read-out strips and the anode–cathode gap, should maximize the signal to noise ratio, according to the analysis of Gatti et al. [4]. Since xenon is a very expensive gas, the MWPC must be sealed or flushed at a very low rate (< 0.3 bubble/second). The chamber was evacuated to 10^{-4} Torr (5 days of pumping) and filled with a mixture of xenon (80%) and CO_2 (20%). The MWPC has been operated for six months with the same gas filling without any significant modification of the working conditions.

Table 2
The MWPC parameters.

Active area	128 $\times$ 128 mm^2
Anode–cathode gap	3.2 mm
Anode wire spacing	2 mm
Anode wire diameter	20 μm
Cathode strips width	2.7 mm
Gas filling	xenon (80%)–CO_2 (20%)
Window thickness	0.18 g/cm^2

4. The read-out electronics

A short examination period is imperative in order to avoid loss of resolution due to patient movements.

Therefore, a primary goal of the read-out system design was to reach a rate capability of a few hundreds kilohertz.

The position read-out system that we adopted (fig. 3) is based on cathode-coupled [5], distributed, home-made, delay-lines (50 ns/cm specific delay, 1600 Ω characteristic impedance) and very fast time to digital converters (LeCroy 4202, $\simeq 500$ ns typical conversion time). The signals at each end of the delay-lines are preamplified with electronic cooled [6] output matching resistors, amplified, and discriminated with a constant fraction technique (CFD ORTEC 583). A very attractive feature of the 4202 TDC is the possibility of measuring positive (the start before the stop) as well as negative (the stop before the start) times. The total delay of the delay-lines is thus reduced by one-half. A pile-up inspector aborts the acquisition of any event which is followed by a second event within a time window of 1 μs. A gateable, presettable timer and counter measures the system dead-time. The anode signal is used only as a gate for the TDCs. A single channel analyzer permits a pulse-height analysis of the anode signal to select the energy window of interest. To by-pass the slow CAMAC cycle and to efficiently store the great amount of data collected in a short time, the most significant seven bits of the first TDC and the most significant eight bits of the second TDC are hardwired on the same output bus to form a 15 bit data word containing the x, y coordinates of an accepted event. The output bus addresses a fast CAMAC histogramming memory (LeCroy 3588). This module acts, in this case, as a two-dimensional multichannel analyzer. The read – increment by one – write cycle of the memory takes only 1.2 μs allowing a data rate of up to 800 kHz. When the acquisition is started, it proceeds independently, so that the computer (Digital

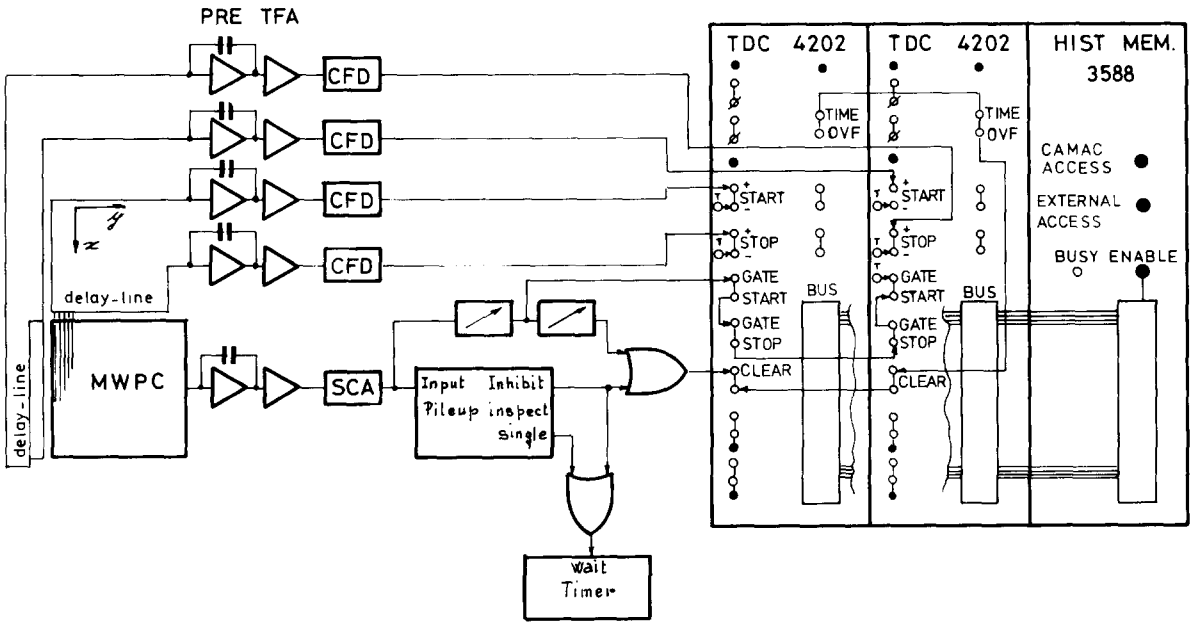

Fig. 3. Block diagram of the position read-out system.

LSI 11-02) can be used to read-out the CAMAC memory and to display the data.

A gray or color real-time image of the X-ray transmission pattern through the object is displayed by means of an image processing system consisting of a matrix of 256×256 pixels, each 10 bits deep. The integral and differential linearity of the electronic chain has been measured to be $\leq 0.5\%$ and $\leq 3\%$, respectively.

5. The MWPC performance

The MWPC was normally operated at 2 atm absolute pressure. At this pressure the detection efficiency is $\simeq 10\%$ for γ's of 45 keV energy. Fig. 4 shows a typical anode pulse-height spectrum at 40 keV. The escape peak (9.5 keV) and the full energy peak (40 keV) are well evident. The energy resolution was $\simeq 30\%$ at this energy and pressure. To study the response to different depositions of energy, the MWPC was exposed to γ's with energies in the interval 20–50 keV. The good linear relationship between energy deposition and pulse-height, as shown in fig. 5, indicates that the chamber is working in the proportional region of gas multiplication.

The most important performance characteristic for imaging applications is, naturally, the spatial resolution. The resolution in the direction orthogonal to the anode wires is set by the wire spacing (2 mm in this case). To measure the spatial resolution in the direction parallel to the anode wires we utilized the PHA wire pattern obtained when there is no sorting in the other direction

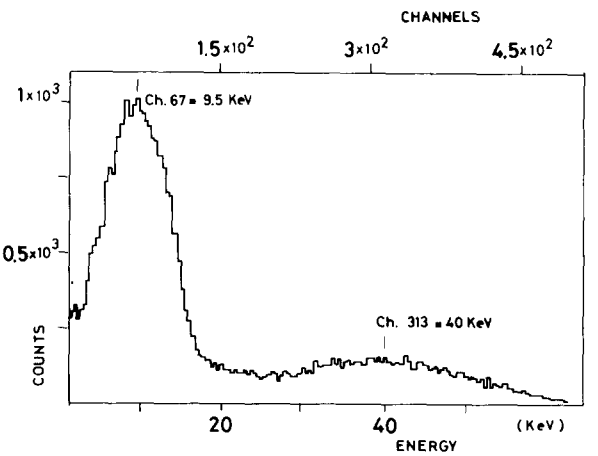

Fig. 4. Anode pulse-height spectrum at 40 keV and 2 atm.

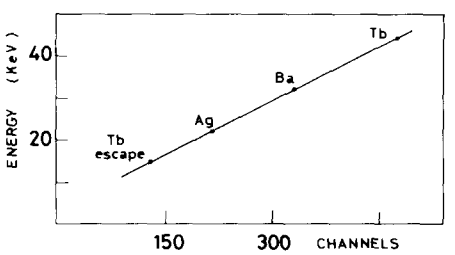

Fig. 5. The linear dependence of the anode pulse-height on energy deposition. Fluorescent X-ray sources were used.

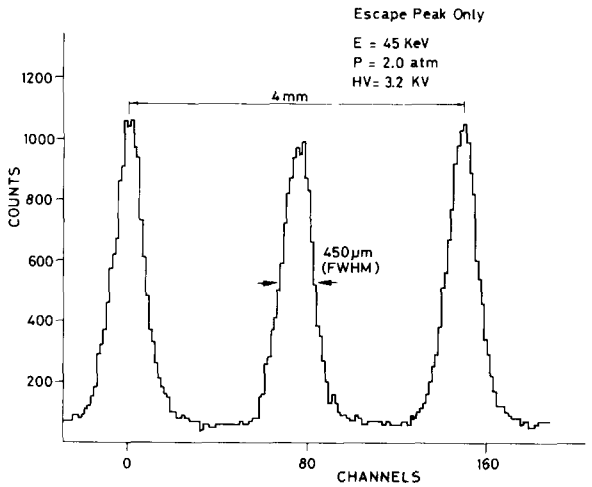

Fig. 6. PHA wire spectrum along the direction orthogonal to the anode wires. Only the events within the escape peak are accepted.

(fig. 6). The wire pitch gives an automatic calibration and the width of the wire "image" is a measure of the resolution along the anode wire. Fig. 7a shows the spatial resolution as a function of HV when only the events falling in the escape peak are accepted. A spatial

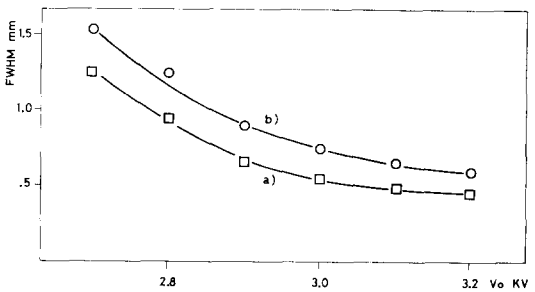

Fig. 7. Curve a): spatial resolution as a function of the operating voltage for events within the escape peak, curve b): the same as a), with all the events accepted.

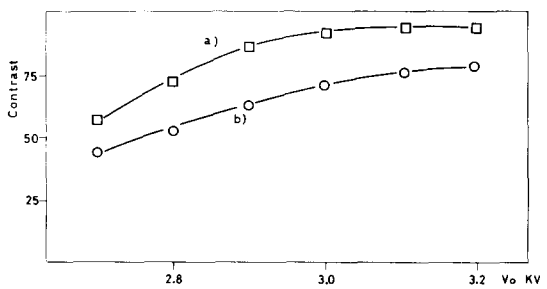

Fig. 8. Curve a): the contrast of the wire pattern as a function of the operating voltage for events within the escape peak, curve b): the same as a), with all the events accepted.

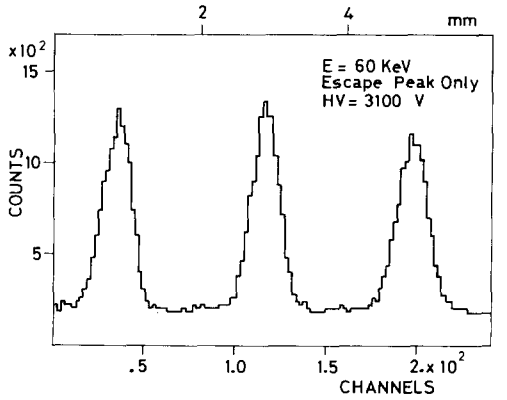

Fig. 9. A wire spectrum obtained with a ^{241}Am source (59.5 keV). Only the events within the escape peak are accepted.

resolution of 450 μm (fwhm) is obtained at a 3.2 kV operating voltage for γ's of 45 keV energy. Because the chamber is operated at 2 atm, the negative effect of the Auger electrons (20% of the cases) and of the photoelectrons resulting from interactions with the xenon

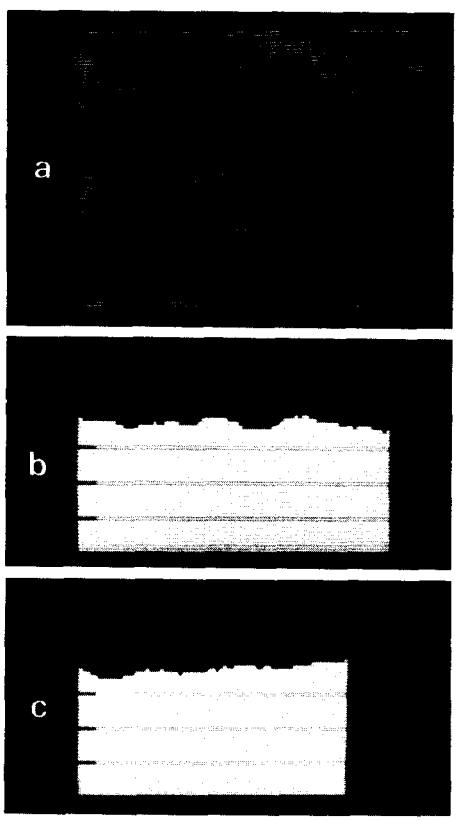

Fig. 10. (a) The response of the system to a uniform illumination, (b) a profile taken along one coordinate, (c) a profile taken along the other coordinate.

Fig. 11. The reconstructed image of two steel nuts separated by 700 μm obtained at 45 keV energy.

L-shell (5% of the cases) on the spatial resolution is strongly reduced. This is shown in fig. 7b where the spatial resolution is plotted as a function of HV with all of the events accepted. A spatial resolution of 750 μm can still be obtained in this case. The negative effect of the Auger or photo-electrons and of the reabsorption of the xenon fluorescent X-ray does not widen the distribution of fig. 5 but adds a tail to the wire structure. Fig. 8 shows the contrast – defined as (Peak − Valley)/(Peak + Valley) – of the wire pattern of fig. 5 as a function of HV for events within the escape peak and for all of the events.

The high gas pressure gives more flexibility to the system. A wider spectrum of energies can be used with a spatial resolution still better than 1 mm. Fig. 9 shows a wire spectrum obtained with a ^{241}Am source (59.5 keV). The spatial resolution is < 1 mm. Fig. 10 shows the response of the MWPC to a uniform illumination together with two profiles taken in the X and Y direction. The wire structure has been suppressed with one-dimensional smoothing. The uniformity is within $\pm 5\%$. In the present configuration (1 μs dead-time) the maximum achievable data rate is 185 kHz, obtained when the true event rate inside the detector is 500 kHz.

6. The imaging capability of the system

To study the imaging capabilities of the system we have imaged several objects with high and low contrast.

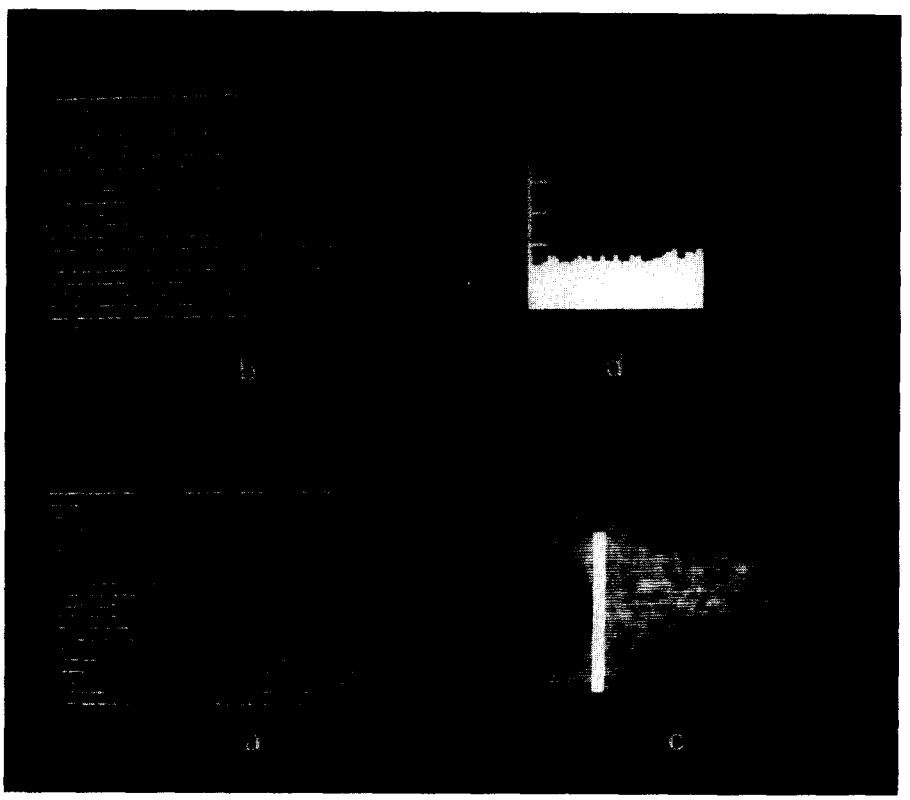

Fig. 12. An example of digital image processing: (a) a transmission pattern through a wrench, (b) a normalization exposure taken, in the same live-time, with the wrench removed from the beam, (c) the two-dimensional distribution of the thickness of the wrench obtained dividing the two images and taking the logarithm of the result, (d) a profile taken along the vertical line shown in (c).

Fig. 11 shows the reconstructed image of two steel nuts of 2 cm outer diameter, separated by 700 μm. Fig. 12 shows an example of the possibilities offered by the digital nature of the reconstructed images. In this case the image of the wrench was divided pixelwise with a normalization exposure made immediately after the first one with the wrench removed and the result scaled down logarithmically. In this way the original image was corrected for inhomogeneities of the system response function and, more significantly, was transformed into an image with a different information content (i.e. the two-dimensional distribution of the wrench thickness). A more difficult problem is to image an object with a very low contrast. Fig. 12 shows an image of a shell that was interposed between the source and the detector. All the significant morphological structures are well resolved.

7. Application of the MWPC to bone densitometry studies

A natural application of this system is in the field of quantitative studies of stationary objects (i.e. body extremities). In this case the measurement can take several seconds without too much discomfort for the patient. At a rate of 100 kHz, 5–10 seconds are more than sufficient to collect statistically significant data, thus minimizing the problem of patient movements.

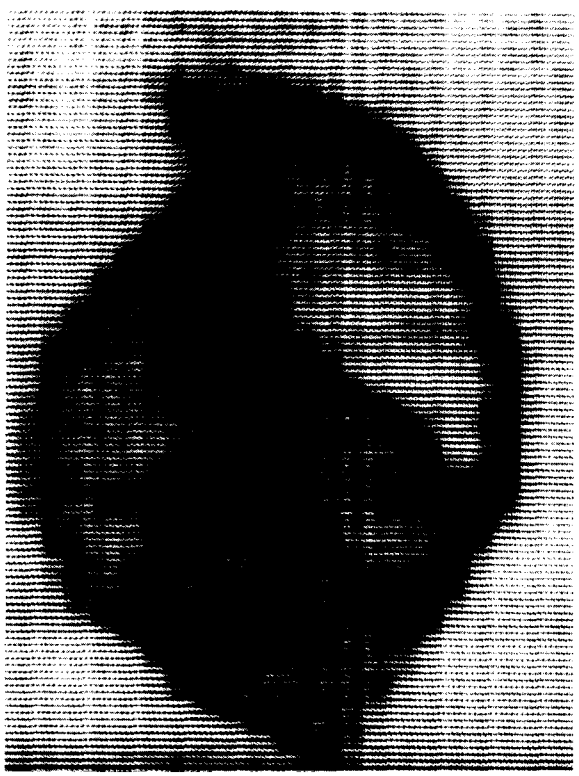

Fig. 13. A MWPC shell radiography.

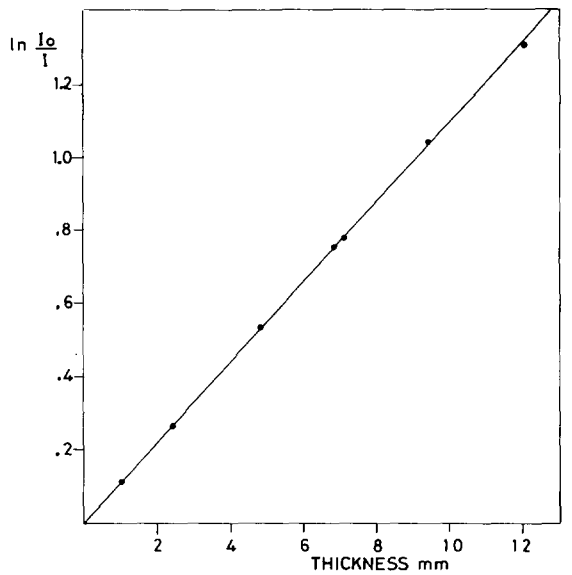

Fig. 14. The mass reconstruction linearity. Horizontal axis: true mass, vertical axis: measured mass.

An interesting application is the direct measurement of bone mass as already introduced by Horsman et al. [7]. In short, the technique is as follows: take a transmission image of a human wrist surrounded by a water bolus; then take a second image of the same water bolus with the sample object removed; divide the two images and take the logarithm of the result. The bone mineral content M is proportional to the sum of the contents of each pixel of the resulting image. The advantages of this

Fig. 15. The two-dimensional bone mass distribution of a wrist of a human skeleton.

technique relative to a scanning arrangement are: i) it is faster; ii) the repositioning accuracy is higher.

We have measured the system linearity, i.e. the response to objects of increasing mass. Several aluminum squares of thicknesses in the interval 1–12 mm were imaged in air and their mass calculated with the technique described above. Fig. 14 shows the resulting linear plot, which indicates that the system is highly linear up to 10 mm thickness. To study the mass resolution an aluminum square of 0.28 mm thickness was added to a 7 mm square. The two different masses were perfectly resolved suggesting that a mass resolution of 1–2% can be obtained. To reduce the scattering problem, especially when the water bolus is utilized, an antiscatter grid (90% rejection power) is inserted between the sample and the MWPC window. Fig. 15 shows an image of the bone mass distribution of the wrist of a human skeleton.

8. Conclusions

The described system has shown an interesting promise for medical imaging applications. It has a submillimeter spatial resolution and a rate capability that can reach the 1 MHz level with faster delay-lines. The digital nature of the resulting images allows extraction of quantitative information from the data and the capability of reaching a much higher sensitivity than conventional X-ray film.

We thank G. Curzio, G. Nicoletti and F. Castellani for providing us with the Ge detector and for their assistance during the X-ray spectra measurements. We thank C. Betti for aid during the setting-up of the electronics and E. Carboni for the careful drawing of the figures.

References

[1] S.E. Bateman et al., Nucl. Instr. and Meth. 135 (1976) 235.
[2] K. Doi et al., Radiology 142 (1982) 233.
[3] R. Bellazzini et al., Nucl. Instr. and Meth., 225 (1984) 145.
[4] E. Gatti et al., Nucl. Instr. and Meth. 163 (1979) 83.
[5] R. Bellazzini et al., Nucl. Instr. and Meth. 190 (1981) 627.
[6] V. Radeka, IEEE Trans. Nucl. Sci. NS-21 (1974) 51.
[7] A. Horsman et al., Phys. Med. Biol. 22 (1977) 1059.